Crystal structure and properties of phosphate $PbCu_2(PO_4)_2$ with spin-singlet ground state

Alexei A. Belik,[1,2,*] Masaki Azuma,[2,3] Akira Matsuo,[4,†] Tomoyuki Kaji,[5] Susumu Okubo,[6,7] Hitoshi Ohta,[6,7] Koichi Kindo,[4,†] and Mikio Takano[2]

[1]*International Center for Young Scientists, National Institute for Materials Science, Namiki 1-1, Tsukuba, Ibaraki 305-0044, Japan*

[2]*Institute for Chemical Research, Kyoto University, Uji, Kyoto-fu 611-0011, Japan*

[3]*PRESTO, Japan Science and Technology Corporation (JST), Kawaguchi, Saitama 332-0012, Japan*

[4]*KYOKUKEN, Osaka University, Toyonaka, Osaka 560-8531, Japan*

[5]*The Graduate School for Science and Technology, Kobe University, Kobe 657-8501, Japan*

[6]*Molecular Photoscience Research Center, Kobe University, Kobe 657-8501, Japan*

[7]*Venture Business Laboratory, Kobe University, Kobe 657-8501, Japan*

(Received 20 October 2005; revised manuscript received 12 December 2005; published 31 January 2006)

Phosphate $PbCu_2(PO_4)_2$ was found in the Pb-Cu-P-O system. Its structure parameters were refined by the Rietveld method using synchrotron x-ray diffraction data [space group *Pccn* (No. 56); $Z=8$; $a=8.03810(10)$ Å, $b=15.46574(14)$ Å, and $c=10.36820(10)$ Å]. $PbCu_2(PO_4)_2$ is isotypic with $SrCu_2(PO_4)_2$. Magnetic properties of $PbCu_2(PO_4)_2$ were investigated by magnetic susceptibility, magnetization up to 65 T, electron-spin resonance, and specific-heat measurements. Magnetic susceptibilities were fit by a linear four-spin cluster model, Cu1-Cu2-Cu2-Cu1 [Hamiltonian: $-2J_1(S_1S_2+S_3S_4)-2J_2S_2S_3$], with $-2J_1/k_B=97.0$ K for Cu1-Cu2 and $-2J_2/k_B=86.5$ K for Cu2-Cu2. The spin gap (Δ/k_B) estimated from the high-field magnetization was 43 K. The g values of $PbCu_2(PO_4)_2$, $g_{//}=2.167$ and $g_{\perp}=2.222$, suggest the $3z^2$-r^2 type of the orbital ground state for Cu^{2+} ions. Specific heat showed that $PbCu_2(PO_4)_2$ does not undergo a long-range magnetic order transition down to 0.45 K in agreement with its spin-singlet ground state.

DOI: 10.1103/PhysRevB.73.024429 PACS number(s): 75.40.Cx, 75.45.+j, 75.50.−y

I. INTRODUCTION

Compounds with a general formula of $AM_2X_2O_n$ (A =alkali-earth elements and Pb; M=divalent transition metals; X=B, P, V, Si, and Ge; n=6–8) have received considerable attention because of their rich and important magnetic properties. For example, $SrCu_2(BO_3)_2$ is a spin gap system that is a physical realization of the Shastry-Sutherland model.[1,2] $PbNi_2(VO_4)_2$ is a Haldane-gap $S=1$ (S is spin) quasi-one-dimensional (1D) antiferromagnet.[3] $BaCu_2(VO_4)_2$ is a compound with a very large spin gap, whose magnetic properties were described by a model of almost isolated dimers (Refs. 4 and 5) and by a 1D bond-alternating chain model.[6,7] $BaCu_2Si_2O_7$ (Refs. 8–10) and $BaCu_2Ge_2O_7$ (Ref. 11) are quasi-1D antiferromagnets with Dzyaloshinskii-Moriya interaction. $BaNi_2(PO_4)_2$ (Refs. 12 and 13) and $BaNi_2(VO_4)_2$ (Ref. 14) are prototypes of a two-dimensional XY system. $SrCu_2(PO_4)_2$ is a realization of a linear four-spin cluster model with a spin gap,[15,16] and a $1/2$-magnetization plateau was observed between 50 and 63 T at 1.3 K.[16] Magnetic properties of $BaCo_2(VO_4)_2$,[17] $BaCo_2Si_2O_7$,[18] and $SrFe_2(PO_4)_2$ (Ref. 19) were also found to be interesting, including, for example, spin-flop and metamagnetic phase transitions.

Among the above compounds, the systems containing ions with $S=1/2$ are particularly of interest because the quantum effects are more enhanced. In the Pb-Cu-P-O system, only two compounds are known so far: $PbCuP_2O_7$,[20] whose magnetic properties are described by a 1D linear chain Heisenberg antiferromagnet model,[21,22] and $Pb_3Cu_3(PO_4)_4$,[23] which is a good realization of a linear Heisenberg antiferromagnetic trimer cluster model.[24,25]

In this work, we report on the preparation and crystal structure refinement of $PbCu_2(PO_4)_2$ belonging to the family of compounds with the general formula of $AM_2X_2O_n$. We characterize this compound by magnetic susceptibility, magnetization up to 65 T, electron-spin resonance (ESR), and specific-heat measurements. Magnetic susceptibilities, high-field magnetization, and specific heat demonstrate the typical behavior for gapped low-dimensional Heisenberg antiferromagnets with a spin-singlet ground state.

II. EXPERIMENTAL

$PbCu_2(PO_4)_2$ was synthesized by the solid-state method at 973 K in air from stoichiometric mixtures of $Pb_3(PO_4)_2$ and $Cu_3(PO_4)_2$ in a Pt crucible for 200 h with five intermediate grindings. The product was cooled in a furnace. It was green-blue in color. The sample contained an impurity of $Pb_3Cu_3(PO_4)_4$ (1.3 mass %).[23] The mass fraction of the impurity in the sample was calculated from scale factors refined in its Rietveld analysis described later. Differential thermal analysis showed two peaks centered at 1068 and 1073 K on heating and two peaks centered at 1022 and 978 K on cooling. This discrepancy of the heating and cooling behaviors suggested that $PbCu_2(PO_4)_2$ melts incongruently above 1060 K. Note that we investigated the whole system $Cu_3(PO_4)_2$-$Pb_3(PO_4)_2$ at 973 K, but only $Pb_3Cu_3(PO_4)_4$ and $PbCu_2(PO_4)_2$ were found. In the $Cu_3(PO_4)_2$-$Sr_3(PO_4)_2$ system, four compounds with interesting magnetic properties exist.[16,24–27]

Single-phased $Cu_3(PO_4)_2$ and $Pb_3(PO_4)_2$ were prepared from mixtures of CuO (99.99%), $NH_4H_2PO_4$ (99.999%), and

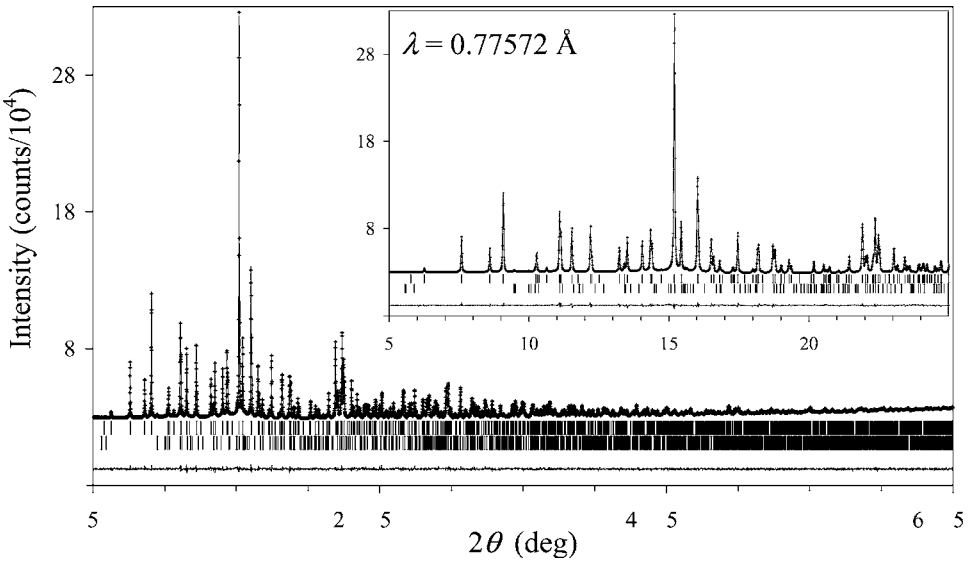

FIG. 1. Observed (crosses), calculated (solid line), and difference synchrotron XRD patterns for $PbCu_2(PO_4)_2$. Bragg reflections are indicated by tick marks for $PbCu_2(PO_4)_2$ (upper) and $Pb_3Cu_3(PO_4)_4$ (lower). Inset shows the enlarged fragment.

PbO (99.9%) by the solid-state method. The mixtures were contained in alumina crucibles, heated under air while raising temperature very slowly from room temperature (RT) to 873 K, reground, and allowed to react at 1153 K for $Cu_3(PO_4)_2$ and 1053 K for $Pb_3(PO_4)_2$ for 120 h with four intermediate grindings.

Synchrotron x-ray powder diffraction (XRD) data of $PbCu_2(PO_4)_2$ were measured at RT on a powder diffractometer BL02B2 at SPring-8 with the Debye-Scherrer geometry.[28] The incident beam from a bending magnet was monochromatized to $\lambda = 0.77572$ Å. The sample was contained in a glass capillary tube with an inner diameter of 0.2 mm and rotated during measurements. The synchrotron XRD data were collected in a 2θ range from 1° to 75° with a step interval of 0.01° during 60 min.

$PbCu_2(PO_4)_2$ was found to be isotypic with $SrCu_2(PO_4)_2$.[16] As initial fractional coordinates in the Rietveld analysis of $PbCu_2(PO_4)_2$, we used those of $SrCu_2(PO_4)_2$. The structure parameters of $PbCu_2(PO_4)_2$ were refined by the Rietveld method from the synchrotron XRD data using RIETAN-2000.[29] The split pseudo-Voigt function of Toraya[30] was used as a profile function. The background was represented by a composite background function, i.e., an 11th-order Legendre polynomial multiplied by a set of numerical values to approximate the background. Coefficients for analytical approximation to atomic scattering factors for Pb, Cu, P, and O were taken from Ref. 31. Isotropic atomic displacement parameters, B, with the isotropic Debye-Waller factor represented as $\exp(-B \sin^2 \theta/\lambda^2)$ were assigned to all the sites.

Magnetic susceptibilities, $\chi = \mathbf{M}/\mathbf{H}$, of $PbCu_2(PO_4)_2$ were measured on a dc SQUID magnetometer (Quantum Design, MPMS XL) between 2 and 400 K in applied fields of 100 and 5000 Oe [1 Oe $= (10^3/4\pi)$ A m^{-1}] under both zero-field-cooled (ZFC) and field-cooled (FC) conditions. Specific heat, $C_p(T)$, was recorded between 0.45 and 31 K on cooling by a pulse relaxation method using a commercial calorimeter (Quantum Design PPMS). High-field magnetization data were taken at 1.3 and 4.2 K in a pulsed magnetic field up to 65 T by an induction method using a multilayer pulse magnet at KYOKUGEN, Osaka University.

The X-band (9.5 GHz) ESR measurements were performed on a powder sample of $PbCu_2(PO_4)_2$ using a Bruker ESR spectrometer EMX081 with a TE_{103} rectangular cavity and an Oxford He flow cryostat ESR900 at Venture Business Laboratory of Kobe University. High-field ESR measurements were done using Gunn oscillators at 80, 160, and 315 GHz and a pulsed magnetic field up to 16 T at Kobe University.[32–35]

III. RESULTS AND DISCUSSION

Figure 1 shows experimental, calculated, and difference synchrotron XRD patterns for $PbCu_2(PO_4)_2$. Structure parameters, lattice parameters, R factors, and so forth are given in Table I, and selected bond lengths, l, and angles, ϕ, in Table II. One of the reasons for the low values of R factors is the high statistics of the synchrotron XRD data (the maximum intensity is 323000 counts).

Cu1 and Cu2 atoms are located in strongly distorted square pyramids. The bases of the pyramids are not flat. The apical Cu2-O31 bond is rather long (about 2.8 Å) and may not be included in the coordination sphere of Cu2 atoms. The $Cu1O_{4+1}$ and $Cu2O_4$ polyhedra are jointed by a vertex (O22) forming a structural dimer unit $Cu1Cu2O_8$. Other Cu-O distances are above 3.0 Å. Therefore, the $Cu1Cu2O_8$ units can be considered as isolated from the structural consideration [Fig. 2(a)].

Figure 3 presents plots of χ and χ^{-1} (ZFC curves) against temperature, T, for $PbCu_2(PO_4)_2$ measured at 100 Oe. No noticeable difference was found between the curves measured under the ZFC and FC conditions. No difference was also observed between curves recorded at 100 and 5000 Oe, except for the lowest temperature range where the $\chi(T)$ curves were determined by impurities or defects. High-temperature regions (150–400 K) were fit very well by the modified Curie-Weiss law,

$$\chi(T) = \chi_0 + \mu_{\text{eff}}^2 N[3k_B(T-\theta)]^{-1}, \quad (1)$$

where χ_0 $[=-1.20(3)\times 10^{-4}$ cm^3/Cu mol$]$ is the temperature-independent term, μ_{eff} $[=1.954(5)\mu_B]$ is the ef-

TABLE I. Fractional coordinates and isotropic atomic displacement parameters for $PbCu_2(PO_4)_2$. Space group *Pccn* (No. 56); $Z=8$; $a=8.03810(10)$ Å, $b=15.46574(14)$ Å, and $c=10.36820(10)$ Å; $R_{wp}=0.89\%$, goodness-of-fit $S=\chi=R_{wp}/R_e=1.66$, $R_p=0.64\%$; $R_B=1.31\%$, and $R_F=1.05\%$ for $PbCu_2(PO_4)_2$; $R_B=1.46\%$, and $R_F=1.09\%$ for the impurity $Pb_3Cu_3(PO_4)_4$ (1.3 mass %).

Atom[a]	Wyckoff position	x	y	z	B (Å^2)
Pb	8*e*	0.02010(6)	−0.12980(3)	−0.08078(5)	0.81(2)
Cu1	8*e*	0.43480(16)	0.16156(9)	−0.05562(16)	0.94(4)
Cu2	8*e*	0.9089(2)	0.07922(11)	−0.2913(2)	1.31(5)
P1	4*d*	0.75	0.25	−0.1766(6)	0.63(11)
P2	8*e*	0.1996(4)	−0.0104(2)	−0.4270(4)	0.15(7)
P3	4*c*	0.25	0.25	0.2074(6)	1.06(14)
O11	8*e*	0.7350(10)	0.1679(4)	−0.2670(8)	0.30(14)
O12	8*e*	0.5907(8)	0.2534(4)	−0.0934(8)	=*B*(O11)
O21	8*e*	0.8803(9)	0.0351(4)	−0.1185(8)	0.07(9)
O22	8*e*	0.6429(8)	0.0805(5)	0.0210(7)	=*B*(O21)
O23	8*e*	0.0824(9)	−0.0070(4)	−0.3122(8)	=*B*(O21)
O24	8*e*	0.2252(7)	0.0737(5)	−0.5035(8)	=*B*(O21)
O31	8*e*	0.4044(10)	0.2230(5)	0.1229(10)	2.8(3)
O32	8*e*	0.3059(10)	0.3304(4)	0.2862(9)	1.0(2)

[a]The occupancies of all the sites are unity.

fective magnetic moment, N is Avogadro's number, k_B is Boltzmann's constant, and θ [=−52.2(7) K] is the Weiss constant.

Below about 150 K, the deviation from the Curie-Weiss law was observed with a broad maximum on the $\chi(T)$ curves at $T_M=55$ K typical for low-dimensional Heisenberg antiferromagnets. Below T_M, the magnetic susceptibilities rapidly decreased, which is characteristic of spin-gapped behavior. The lowest-temperature region (below about 10 K) was characterized by an increase in the χ values due to the presence of impurities or defects.

Taking into account the presence of the structural $Cu1Cu2O_8$ dimer units, the $\chi(T)$ data in the whole range of temperatures of 2–400 K were first fit by the dimer model,

$$\chi(T)=\chi_0+C_{\text{imp}}/(T-\theta_{\text{imp}})+\chi_{\text{spin}}(T), \tag{2}$$

$$\begin{aligned}\chi_{\text{spin}}(T)&=\chi_{\text{dimer}}(T)\\&=Ng^2\mu_B^2(k_BT)^{-1}\{3+\exp[-2J/(k_BT)]\}^{-1}\\&\quad\text{with Hamiltonian}\\&\quad H_{\text{dimer}}=-2J(S_1S_2),\end{aligned} \tag{3}$$

where C_{imp} is an impurity Curie constant, θ_{imp} is an impurity Weiss constant, g is the spectroscopic splitting factor (g factor), and $-2J$ is the exchange constant in the dimer unit. However, in the dimer model, the fit was not good (Fig. 3 and Table III) and the g value was too small if refined ($g=1.90$), whereas the EPR experiments gave $g_{\text{av}}=2.19$ for $PbCu_2(PO_4)_2$. This fact indicated that this model is incorrect. Then we tried to include the interdimer interaction (zJ') by means of a mean-field approximation,[36]

$$\chi_{\text{spin}}(T)=Ng^2\mu_B^2(k_BT)^{-1}\{3+\exp[-2J/(k_BT)]+zJ'/(k_BT)\}^{-1}. \tag{4}$$

However, the fit gave the large value of zJ'/k_B (Table III) apparently beyond the validity of a mean-field approximation ($|J'|\ll|J|$).

Therefore, other interactions between Cu^{2+} ions should be taken into account. These are Cu-O···O-Cu super-superexchange interactions, where O···O is an edge of a PO_4 group. Twelve such Cu-Cu interactions mediated by Cu-O···O-Cu paths [Fig. 2(b)] can be found in $PbCu_2(PO_4)_2$. The spin dimer analysis (Refs. 22, 37, and 38) in the case of $SrCu_2(PO_4)_2$ showed that the two strongest spin exchange interactions between Cu sites arise from the Cu1-O···O-Cu2 and Cu2-O···O-Cu2 super-superexchange paths marked by J_1 and J_2, respectively, in Fig. 2(b); the superexchange associated with the structural dimer $Cu1Cu2O_8$ is negligible.[16] These Cu sites connected with the super-superexchange paths J_1 and J_2 form a linear four-spin cluster unit, Cu1-Cu2-Cu2-Cu1. Therefore, we analyzed the magnetic susceptibility data of $PbCu_2(PO_4)_2$ using a linear four-spin cluster model [Eqs. (2), (5), and (6)],[39,40]

$$\begin{aligned}\chi_{\text{spin}}(T)&=\chi_{\text{linear-tetramer}}(T)\\&=\frac{Ng^2\mu_B^2}{3k_BT}\frac{\sum_i S_i(S_i+1)(2S_i+1)\exp\left(-\frac{E_i}{k_BT}\right)}{\sum_i (2S_i+1)\exp\left(-\frac{E_i}{k_BT}\right)}\end{aligned}$$

with the Hamiltonian

TABLE II. Bond lengths, l, and angles, ϕ, in $PbCu_2(PO_4)_2$.

	l (Å) and ϕ (deg)
Pb-O11	2.413(8)
Pb-O31	2.498(8)
Pb-O24	2.671(6)
Pb-O21	2.656(8)
Pb-O12	2.616(7)
Pb-O21'	2.814(6)
Pb-O32	2.807(8)
Pb-O22	2.882(7)
Pb-O23	3.100(7)
Cu1-O24	1.947(7)
Cu1-O12	1.934(6)
Cu1-O32	1.944(9)
Cu1-O31	2.094(10)
Cu1-O22	2.237(7)
Cu1-O23	3.000(7)
Cu2-O11	1.974(7)
Cu2-O23	1.942(7)
Cu2-O21	1.930(8)
Cu2-O22	1.990(7)
Cu2-O31	2.826(8)
Cu2-O23'	3.047(8)
Cu1-O31-Cu2	81.9(3)
Cu1-O22-Cu2	101.3(3)
P1-O11 (×2)	1.583(8)
P1-O12 (×2)	1.545(8)
P2-O21	1.574(7)
P2-O22	1.527(8)
P2-O23	1.519(8)
P2-O24	1.538(8)
P3-O31 (×2)	1.576(9)
P3-O32 (×2)	1.554(8)

$$H_{\text{linear-tetramer}} = -2J_1(S_1S_2 + S_3S_4) - 2J_2S_2S_3. \quad (5)$$

The eigenvalues of the Hamiltonian are as follows:

$$E_1(S=2) = -J_1 - J_2/2,$$

$$E_2(S=1) = J_1 - J_2/2,$$

$$E_3(S=1) = J_2/2 + \sqrt{J_1^2 + J_2^2},$$

$$E_4(S=1) = J_2/2 - \sqrt{J_1^2 + J_2^2},$$

$$E_5(S=0) = J_1 + J_2/2 + \sqrt{4J_1^2 - 2J_1J_2 + J_2^2},$$

$$E_6(S=0) = J_1 + J_2/2 - \sqrt{4J_1^2 - 2J_1J_2 + J_2^2}. \quad (6)$$

The fitting parameters are summarized in Table III and the resulting curve is shown in Fig. 3. The first excited energy, $\Delta_1/k_B = E_4 - E_6$, in this model is 67.7 K.

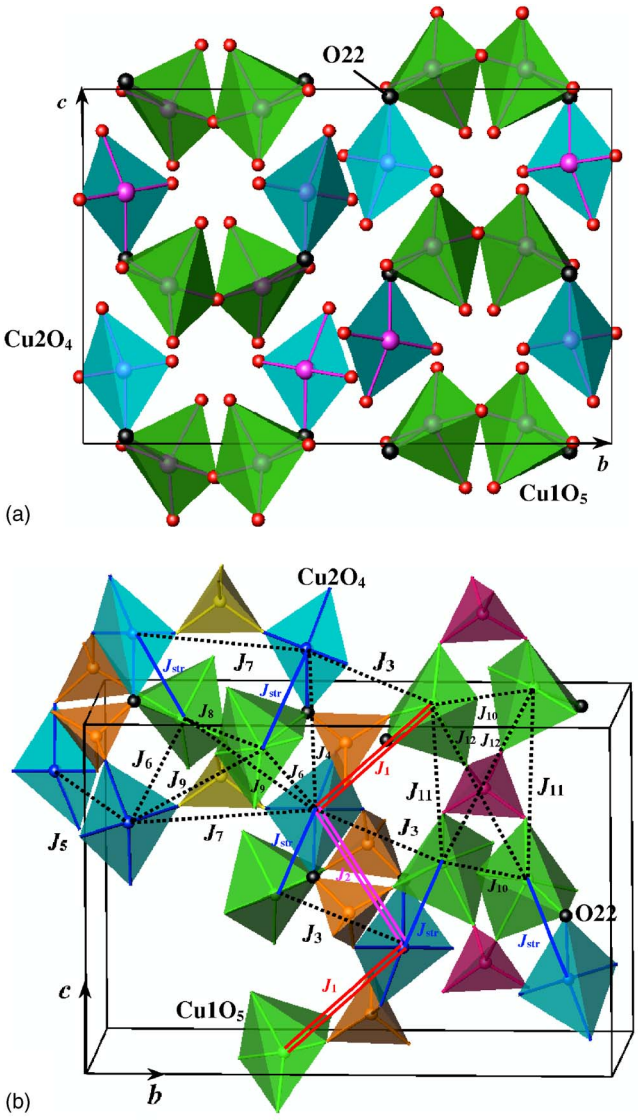

FIG. 2. (Color online) (a) Projection of the structure of $PbCu_2(PO_4)_2$ along the a axis showing the arrangement of $Cu1O_{4+1}$ and $Cu2O_4$ polyhedra. (b) Fragment of the structure of $PbCu_2(PO_4)_2$ emphasizing the connections between Cu atoms transferred through PO_4 groups, J_1–J_{12}. J_{str} denotes the structural dimer unit. J_1 and J_2 are shown by the double lines.

High-field isothermal magnetization data, M versus H, at 1.3 K are presented in Fig. 4. The small change of the magnetization below about 30 T is due to the presence of paramagnetic impurities. Above $H_1 \approx 29.5$ T, the magnetization rapidly increased and changed almost linearly with the field up to 65 T. In $SrCu_2(PO_4)_2$, a curvature near $H_2 = 50$ T was observed (Fig. 4) with the magnetization value of about half the expected saturation value.[16] Probably the magnetic field of 65 T was not enough to observe a magnetization plateau in $PbCu_2(PO_4)_2$. The spin gap can be estimated using the equation

$$\Delta/k_B = 0.6714 g H_1. \quad (7)$$

This equation gives $\Delta/k_B \approx 43$ K. The values of H_1 were almost the same in $SrCu_2(PO_4)_2$ and $PbCu_2(PO_4)_2$. However,

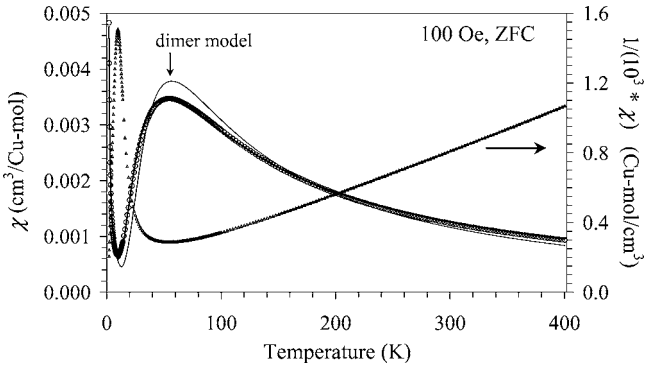

FIG. 3. The $\chi(T)$ and $\chi^{-1}(T)$ curves for the powder $PbCu_2(PO_4)_2$ sample. Solid line on the $\chi^{-1}(T)$ curve is the fit to Eq. (1) at 150–400 K. Solid lines on the $\chi(T)$ curves are the fits by the dimer and linear-four-spin cluster models. Parameters of the fitting are presented in Table III.

the slope of the M versus H curves was different after H_1 for $SrCu_2(PO_4)_2$ and $PbCu_2(PO_4)_2$, probably due to different intercluster interactions.

The interaction between Cu^{2+} ions in $PbCu_2(PO_4)_2$ is rather complex [Fig. 2(b)]. The linear four-spin cluster model takes into account only the two strongest interactions. This is

TABLE III. Fitted parameters for $\chi(T)$ of $PbCu_2(PO_4)_2$.

Equations	Quantity	Value
(2) and (3) dimer model	Temperature range (K)	2–400
	χ_0 (cm^3/Cu mol)	$-2.4(2)\times10^{-4}$
	C_{imp} (cm^3 K/Cu mol)	$7.4(4)\times10^{-3}$
	θ_{imp} (K)	0.37(11)
	g[a]	2.19 (fixed)
	$-2J/k_B$ (K)	93.1(7)
	R[b]	1.04×10^{-2}
(2) and (4) dimer model with the interdimer interaction by means of a mean-field approximation	Temperature range (K)	2–400
	χ_0 (cm^3/Cu mol)	$0.0(9)\times10^{-5}$
	C_{imp} (cm^3 K/Cu mol)	$4.93(9)\times10^{-3}$
	θ_{imp} (K)	0.96(3)
	g[a]	2.19 (fixed)
	$-2J/k_B$ (K)	82.3(3)
	zJ'/k_B (K)	119(3)
	R[b]	1.11×10^{-3}
(2), (5), and (6) linear four-spin cluster model	Temperature range (K)	2–400
	χ_0 (cm^3/Cu mol)	$-7.9(4)\times10^{-5}$
	C_{imp} (cm^3 K/Cu mol)	$5.19(5)\times10^{-3}$
	θ_{imp} (K)	0.926(15)
	g[a]	2.19 (fixed)
	$-2J_1/k_B$ (K)	97.0(2)
	$-2J_2/k_B$ (K)	86.5(7)
	R[b]	3.29×10^{-4}

[a]The g parameter was fixed at the value determined from the ESR measurements.

[b]$R=\sum_{i=1}^{N_p}[\chi(T_i)-\chi_{fit}(T_i)]^2 \Big/ \sum_{i=1}^{N_p}[\chi(T_i)]^2$

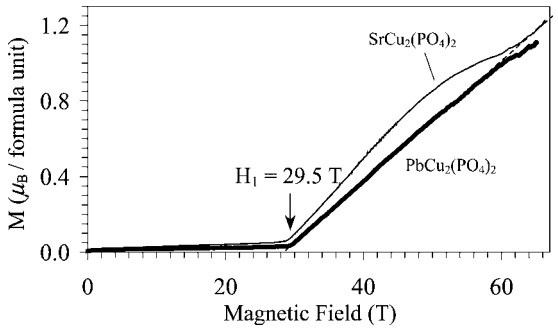

FIG. 4. High-field magnetization curves at 1.3 K for powder $PbCu_2(PO_4)_2$ and $SrCu_2(PO_4)_2$ given for comparison.

why the spin gap deduced from the linear four-spin cluster model (indirect method) does not coincide with the spin gap deduced from the high-field magnetization data. To determine the strength of other interactions, additional information is needed. For example, first-principles calculations can provide such information (Ref. 41) or inelastic neutron scattering experiments (Ref. 40) will give important information about the excitation spectrum of $PbCu_2(PO_4)_2$.

The specific heat exhibited no anomaly characteristic of a long-range order except for a very small peak at 1.3 K due to the long-range magnetic order in the impurity, $Pb_3Cu_3(PO_4)_4$.[24] These data evidenced that $PbCu_2(PO_4)_2$ does not undergo a magnetic transition down to 0.45 K. This fact is in accordance with a spin-singlet ground state of $PbCu_2(PO_4)_2$.

Figure 5 shows the results of the X-band ESR measurements for $PbCu_2(PO_4)_2$. The temperature dependence of the integrated intensity was similar to the magnetic susceptibility, but no upturn was observed down to 4.2 K. These results suggested that the observed ESR signals are intrinsic to the sample down to 4.2 K. However, the effect of impurities does exist in the ESR results, because the integrated intensities did not tend to zero at low temperatures. The increase of the g value was observed below 50 K, which corresponds to the maximum of the magnetic susceptibility. Therefore, the observed g shift may be related to the development of some correlations in the system. Because it was difficult to resolve

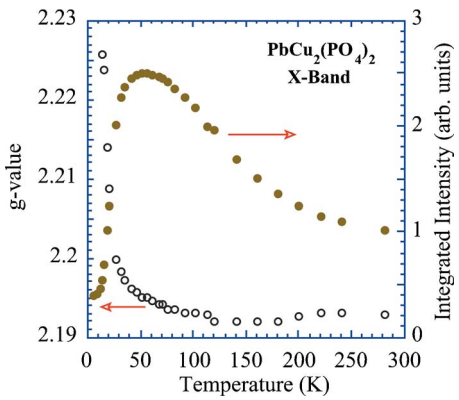

FIG. 5. (Color online) Temperature dependences of g value and the integrated intensity of the powder $PbCu_2(PO_4)_2$ sample observed by the X-band ESR measurements.

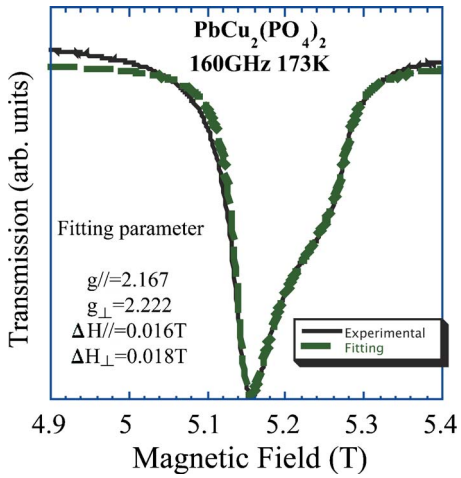

FIG. 6. (Color online) Typical absorption lines observed at 160 GHz for the powder $PbCu_2(PO_4)_2$ sample. The line-shape analysis (the broken line) is performed. The details can be seen in the text.

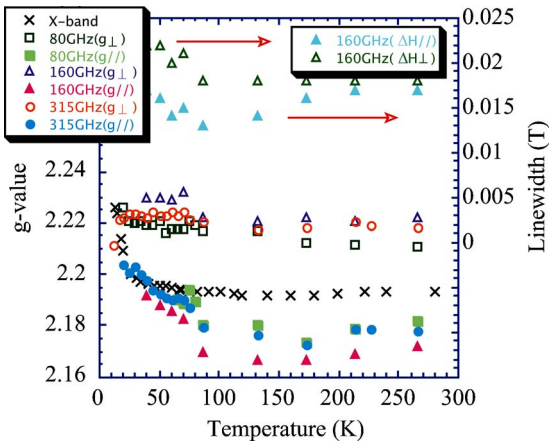

FIG. 7. (Color online) The g values and linewidths of the powder $PbCu_2(PO_4)_2$ sample as a function of temperature. The g values and linewidths for 160 GHz are obtained by the line-shape analyses as shown in Fig. 6.

the anisotropic g values in the X-band measurements, we performed the high-field ESR measurements.

Figure 6 shows typical absorption lines observed at 160 GHz for $PbCu_2(PO_4)_2$. The anisotropic g values were resolved in this case. The powder absorption spectra for $PbCu_2(PO_4)_2$ were analyzed by the following equations (Ref. 35) as shown in Fig. 6 by the broken line:

$$I(H) = -\int \frac{A \sin\theta}{(h\nu - g\mu_B H)^2 + B^2} d\theta, \tag{8}$$

where $g = \sqrt{(g_\perp \sin\theta)^2 + (g_{//}\cos\theta)^2}$ and $B = \sqrt{(g_\perp \mu_B \Delta H_\perp \sin\theta)^2 + (g_{//}\mu_B \Delta H_{//}\cos\theta)^2}$.

The g values of $g_{//}=2.167$ and $g_\perp=2.222$ in $PbCu_2(PO_4)_2$ suggest the $3z^2$-r^2 type of the orbital ground state for Cu^{2+} ions because $g_{//}<g_\perp$, while $g_{//}>g_\perp$ for the x^2-y^2 type of the orbital ground state.[42] The $3z^2$-r^2 type of the orbital ground state seems to be also reasonable for the strongly distorted square pyramid crystal field in $PbCu_2(PO_4)_2$. However, the $g_{//}$ value should be close to 2 in the case of the $3z^2$-r^2 ground state, and the obtained g values cannot be interpreted completely by a Cu^{2+} ion site. In order to understand the g values in $PbCu_2(PO_4)_2$, the exchange narrowing among more than two different g-tensor Cu^{2+} ion sites should be considered. Therefore, the experimental results of high-field ESR measurements supported the model with multi-Cu^{2+} ion sites connected by the exchange interactions. Figure 7 shows the temperature dependence of g values and the linewidth of $PbCu_2(PO_4)_2$. It is clear that the dynamical property changes at low temperatures. However, it is not clear at the moment why the $g_{//}$ value approaches the value of about 2.22 at low temperatures. In order to clarify this point, more detailed high-field ESR measurements using single crystals are required.

In conclusion, the crystal structure and properties of $PbCu_2(PO_4)_2$, belonging to the family of compounds with the general formula of $AM_2X_2O_n$, were investigated. Magnetic susceptibilities, high-field magnetization, and specific heat showed that $PbCu_2(PO_4)_2$ has a spin-singlet ground state. Magnetic susceptibilities of $PbCu_2(PO_4)_2$ were described by the linear four-spin cluster model.

ACKNOWLEDGMENTS

The authors express their thanks to the Ministry of Education, Culture, Sports, Science and Technology, Japan, for Grant-in-Aid No. 12CE2005, for COE Research on Elements Science (No. 13440111 and No. 14204070), and for 21COE on the Kyoto Alliance for Chemistry. ICYS is supported by Special Coordination Funds for Promoting Science and Technology from MEXT, Japan.

*Author to whom correspondence should be addressed. Email address: Alexei.BELIK@nims.go.jp

†Present address: Institute for Solid State Physics, University of Tokyo, Kashiwanoha 5-1-5, Kashiwa, Chiba 277-8581, Japan.

[1] H. Kageyama, K. Yoshimura, R. Stern, N. V. Mushnikov, K. Onizuka, M. Kato, K. Kosuge, C. P. Slichter, T. Goto, and Y. Ueda, Phys. Rev. Lett. **82**, 3168 (1999).

[2] K. Kodama, M. Takigawa, M. Horvatic, C. Berthier, H. Kageyama, Y. Ueda, S. Miyahara, F. Becca, and F. Mila, Science **298**, 395 (2002).

[3] Y. Uchiyama, Y. Sasago, I. Tsukada, K. Uchinokura, A. Zheludev, T. Hayashi, N. Miura, and P. Böni, Phys. Rev. Lett. **83**, 632 (1999).

[4] H. Sakurai, K. Yoshimura, and K. Kosuge, J. Phys. Soc. Jpn., Suppl. **71**, 190 (2002).

[5] C. S. Lue and B. X. Xie, Phys. Rev. B **72**, 052409 (2005).

[6] Z. He, T. Kyomen, and M. Itoh, Phys. Rev. B **69**, 220407(R) (2004).
[7] K. Ghoshray, B. Pahari, B. Bandyopadhyay, R. Sarkar, and A. Ghoshray, Phys. Rev. B **71**, 214401 (2005).
[8] I. Tsukada, Y. Sasago, K. Uchinokura, A. Zheludev, S. Maslov, G. Shirane, K. Kakurai, and E. Ressouche, Phys. Rev. B **60**, 6601 (1999).
[9] I. Tsukada, J. Takeya, T. Masuda, and K. Uchinokura, Phys. Rev. Lett. **87**, 127203 (2001).
[10] A. Zheludev, M. Kenzelmann, S. Raymond, E. Ressouche, T. Masuda, K. Kakurai, S. Maslov, I. Tsukada, K. Uchinokura, and A. Wildes, Phys. Rev. Lett. **85**, 4799 (2000).
[11] P. Gaveau, J. P. Boucher, L. P. Regnault, and Y. Henry, J. Appl. Phys. **69**, 6228 (1991).
[12] M. Heinrich, H. A. Krug von Nidda, A. Loidl, N. Rogado, and R. J. Cava, Phys. Rev. Lett. **91**, 137601 (2003).
[13] N. Rogado, Q. Huang, J. W. Lynn, A. P. Ramirez, D. Huse, and R. J. Cava, Phys. Rev. B **65**, 144443 (2002).
[14] S. Bertaina, V. A. Pashchenko, A. Stepanov, T. Masuda, and K. Uchinokura, Phys. Rev. Lett. **92**, 057203 (2004).
[15] M. Mekata, T. Hanabata, K. Nakaya, and Y. Ajiro, J. Magn. Magn. Mater. **226-230**, 410 (2001).
[16] A. A. Belik, M. Azuma, A. Matsuo, M. -H. Whangbo, H. -J. Koo, J. Kikuchi, T. Kaji, S. Okubo, H. Ohta, K. Kindo, and M. Takano, Inorg. Chem. **44**, 6632 (2005).
[17] Z. He, D. Fu, T. Kyomen, T. Taniyama, and M. Itoh, Chem. Mater. **17**, 2924 (2005).
[18] R. D. Adams, R. Layland, C. Payen, and T. Datta, Inorg. Chem. **35**, 3492 (1996).
[19] A. A. Belik, M. Azuma, M. Takano, and B. I. Lazoryak, Chem. Mater. **16**, 4311 (2004).
[20] A. Elmarzouki, A. Boukhari, E. M. Holt, and A. Berrada, J. Alloys Compd. **227**, 125 (1995).
[21] A. A. Belik, M. Azuma, and M. Takano, Inorg. Chem. **42**, 8572 (2003).
[22] H. -J. Koo, D. Dai, and M. -H. Whangbo, Inorg. Chem. **44**, 4359 (2005).
[23] H. Effenberger, J. Solid State Chem. **142**, 6 (1999).
[24] A. A. Belik, A. Matsuo, M. Azuma, K. Kindo, and M. Takano, J. Solid State Chem. **178**, 709 (2005).
[25] M. Matsuda, K. Kakurai, A. A. Belik, M. Azuma, M. Takano, and M. Fujita, Phys. Rev. B **71**, 144411 (2005).
[26] A. A. Belik, A. P. Malakho, B. I. Lazoryak, and S. S. Khasanov, J. Solid State Chem. **163**, 121 (2002).
[27] A. A. Belik, S. Uji, T. Terashima, and E. Takayama-Muromachi, J. Solid State Chem. **178**, 3461 (2005).
[28] E. Nishibori, M. Takata, K. Kato, M. Sakata, Y. Kubota, S. Aoyagi, Y. Kuroiwa, M. Yamakata, and N. Ikeda, Nucl. Instrum. Methods Phys. Res. A **467-468**, 1045 (2001).
[29] F. Izumi and T. Ikeda, Mater. Sci. Forum **321-324**, 198 (2000).
[30] H. Toraya, J. Appl. Crystallogr. **23**, 485 (1990).
[31] *International Tables for Crystallography*, Vol. C, 2nd ed., edited by A. J. C. Wilson and E. Prince (Kluwer, Dordrecht, 1999), pp. 572–574.
[32] M. Motokawa, H. Ohta, and N. Makita, Int. J. Infrared Millim. Waves **12**, 149 (1991).
[33] N. Nakagawa, T. Yamada, K. Akioka, S. Okubo, S. Kimura, and H. Ohta, Int. J. Infrared Millim. Waves **19**, 167 (1998).
[34] H. Ohta, S. Okubo, T. Sakurai, T. Goto, K. Kirita, K. Ueda, Y. Uwatoko, T. Saito, M. Azuma, M. Takano, and J. Akimitsu, Physica B **294-295**, 624 (2001).
[35] H. Ohta, S. Kimura, and M. Motokawa, J. Phys. Soc. Jpn. **64**, 3934 (1995).
[36] Y. Sasago, M. Hase, K. Uchinokura, M. Tokunaga, and N. Miura, Phys. Rev. B **52**, 3533 (1995).
[37] M. -H. Whangbo, H. -J. Koo, and D. Dai, J. Solid State Chem. **176**, 417 (2003).
[38] M. -H. Whangbo, D. Dai, and H. -J. Koo, Solid State Sci. **7**, 827 (2005).
[39] A. N. Papadopoulos, A. Tangoulis, C. P. Raptopoulou, A. Terzis, and D. P. Kessissoglou, Inorg. Chem. **35**, 559 (1996).
[40] M. Hase, K. M. S. Etheredge, S. -J. Hwu, K. Hirota, and G. Shirane, Phys. Rev. B **56**, 3231 (1997).
[41] R. Valentí, T. Saha-Dasgupta, and C. Gros, Phys. Rev. B **66**, 054426 (2002).
[42] A. Abragam and B. Bleaney, *Electron Paramagnetic Resonance of Transition Ions* (Clarendon Press, Oxford, 1970), p. 456.